

Synthesis of samarium doped gadolinium oxide nanorods, its spectroscopic and physical properties

G Boopathi¹, S Gokul Raj², G Ramesh Kumar³, R Mohan¹ and S Mohan^{4*}

¹Department of Physics, Presidency College, Chennai 600 005, India

²Department of Physics, C. Kandaswami Naidu College for Men, Anna Nagar, Chennai 600 102, India

³Department of Physics, University College of Engineering Arni, Anna University Chennai, Arni 632 317, India

⁴School of Science and Humanities, Vel Tech University, Avadi, Chennai 600 062, India

Received: 26 July 2017 / Accepted: 07 October 2017 / Published online: 26 December 2017

Abstract: One-dimensional samarium doped gadolinium oxide [Sm:Gd₂O₃] nanorods have been synthesized successfully through co-precipitation technique in aqueous solution. The as-synthesized and calcined products were characterized by using powder X-ray diffraction pattern, Fourier transform Raman spectroscopy, thermogravimetric/differential thermal analysis, scanning electron microscopy with energy-dispersive X-ray analysis, transmission electron microscopy, Fourier transform infrared spectroscopy, Ultraviolet–Visible spectrometry, photoluminescence spectrophotometer and X-ray photoelectron spectroscopy techniques. The obtained results are discussed in detailed manner.

Keywords: One-dimensional (1D) nanorods; Samarium doped gadolinium oxide; TEM; XPS; Thermal analysis; Rare earth oxides

PACS Nos.: 64.70 Ja; 78.30-j

1. Introduction

The lanthanide sesquioxides (Ln₂O₃) are currently of considerable interest across a large range of scientific disciplines as a consequence of their unique structural, optical and electronic properties. They are technologically important for several optical applications including X-ray imaging [1], field emission and electroluminescent displays [2], optical amplifiers [3] and sensing technologies [4]. There are extensive studies on the synthesis of 1-D rod-, wire- or tube-like lanthanide compounds including lanthanide hydroxide (Ln(OH)₃) and lanthanide oxide (Ln₂O₃) by various methods [5–7]. The doping of lanthanide oxide with another rare-earth cation is a rapidly emerging area for fluorescent labeling for immunoassays, with the oxides exhibiting narrow emission spectra, long luminescence lifetime and low toxicity [8]. Rare-earths (RE) are well known for their extensive use in luminescent materials. The

RE³⁺ ions doped inorganic nanophosphor is one of the most promising materials for a variety of applications in solid-state lasers (SSL), lighting, displays such as fluorescent lamps, cathode ray tubes (CRT) and field emission displays (FED) and optical communication fields. There is a growing interest in the study of inorganic nanocrystals doped with trivalent lanthanide ions (RE³⁺) due to their wide range of industrial applications such as electronic and photonic devices and amplification in optical communications, luminescent thermometers, fluorescent and magnetic resonance imaging and bio-labeling [9].

An improved performance of displays and lamps requires high quality of phosphors for sufficient brightness and long-term stability. In practice, a densely packed layer of small size particles can improve aging problems. On the other hand, when the particle is smaller than the critical value, then the luminescence efficiency decreases due to the increased light reabsorption and the luminescence quenching by the surface layer. Thus, high-concentration of surface defects and microstrains could greatly reduce the total luminescent intensity of nanosized luminescent materials. The concentration quenching of activators

*Corresponding author, E-mail: smoh1947@rediffmail.com

ranges are also different from those of corresponding bulk materials [10]. As a consequence of their structural flexibility, doped sesquioxides have potential applications in nuclear engineering, oxygen-ion conductors for use in solid oxide fuel cells (SOFC), oxygen sensors, dense ceramic membranes for oxygen separation and membrane reactors for oxidative catalysis [11]. Added to this, nanoparticles of lanthanide oxides are promising candidates in biotechnology due to their optical properties such as large Stokes shift, lack of photobleaching and long fluorescence lifetime (~ 1 ms). The large Stokes shift allows the subtraction of the excitation wavelength by filtering while the long lifetime allows for time-gated detection and subtraction of the background fluorescence [8]. In general, lanthanide oxides, Ln_2O_3 , exhibit three main crystal structures viz, hexagonal, cubic and monoclinic [12, 13]. Cubic Gd_2O_3 contains two nonequivalent cation sites, C_2 (noncentrosymmetric) and S_6 (centrosymmetric), in 3:1 ratio.

Samarium (Sm^{3+}) ions were used as dopant and that Sm^{3+} has a complex energy level structure with ground $6H_J$ and $6F_J$ multiplets and related fluorescence can be observed in the visible and near-infrared range [14, 15]. Sm^{3+} is an ion with an odd number of electrons in its 4f shell. Placed inside a solid, the electric field of the surrounding ions lifts the degeneracy of the free ion 4f electronic states and leads to a new set of levels. All levels are at least twofold degenerate as a consequence of Kramers theorem [16]. In the present study, samarium doped gadolinium oxide ($\text{Sm}:\text{Gd}_2\text{O}_3$) nanorods were produced through the heat treatments of 500, 750 and 1000 °C for 1 h by using the corresponding hydroxides as the precursors. The synthesis conditions, such as concentration of dopant ions and calcination time and temperature, may change the RE^{3+} ions radiative lifetimes and the mechanisms of energy-transfer between ions located in sites with different local symmetry.

Many luminescent particles of different chemical compositions, shapes and size distributions have been prepared by different methods [17]. Recently, different morphological Ln_2O_3 materials were prepared by hydrothermal method, sol-gel technology, spray pyrolysis, combustion reaction and chemical vapor deposition method [18]. The nanostructure formed depends on the pressure, template or surfactant and catalysts. But this results in experimental complexity, impurities, defects and high cost. In addition, these methods could not meet large scale produce in industry. Among other preparation methods, co-precipitation technique does not require the use of template or surfactant. It is a promising technique to gain a mass production.

In the present investigation, an attempt has been made to synthesize samarium doped gadolinium hydroxide ($\text{Sm}:\text{Gd}(\text{OH})_3$) successfully by co-precipitation technique,

in which ammonium hydroxide was used as the alkali agent. As synthesized and calcined products were characterized by using powder XRD pattern, FT-Raman spectroscopy, TG/DTA analyzer, SEM/EDX instrument, TEM instrument, FT-IR spectroscopy, UV-Vis spectrophotometer, PL spectrophotometer and XPS instrument. The structural, morphological and optical properties of hydroxide and oxide nanophosphors were investigated and discussed in detail.

2. Experimental details

2.1. Materials used

The starting materials used for preparation of $\text{Sm}:\text{Gd}_2\text{O}_3$ nanorods were of analytical grade. Gadolinium nitrate hexahydrate [$\text{Gd}(\text{NO}_3)_3 \cdot 6\text{H}_2\text{O}$ (Alfa Aesar, purity 99.99%)] used as host/oxidizer, samarium nitrate hexahydrate [$\text{Sm}(\text{NO}_3)_3 \cdot 6\text{H}_2\text{O}$ (Alfa Aesar, purity 99.99%)] used as dopant, ammonium hydroxide [NH_4OH (99%)] was used as a buffer solution and doubly-distilled water was used as a solvent. All chemicals were used as such without further purification.

2.2. Preparation of $\text{Sm}:\text{Gd}_2\text{O}_3$ nanorods

The cubic phase $\text{Sm}:\text{Gd}_2\text{O}_3$ nanorods were obtained via co-precipitation technique. In a typical synthesis, 100 mL of double-distilled water solvent containing 4.194 mmol of $\text{Gd}(\text{NO}_3)_3 \cdot 6\text{H}_2\text{O}$ and 0.276 mmol of $\text{Sm}(\text{NO}_3)_3 \cdot 6\text{H}_2\text{O}$ were used as starting materials. The doping percentage of samarium was maintained to 5 at.%. The above mentioned chemical mixture were placed over a magnetic stirrer. The magnetic stirrer was stirred vigorously for about 1 h. The reaction temperature was maintained at a temperature of 60 °C for 1 h. The pH value of the solution at this level was noted down to be 6 during the period of 1 h reaction time. After 1 h of reaction, the magnetic stirrer was switched off. Then, in order to obtain the precipitation, approximately 25 mL of NH_4OH (0.178 mol) solution was added to the stirred chemicals mixture. Now the pH value of this solution was again noted down to be around 13. For decreasing the pH value of the solution, the double-distilled water was added excessively by several times. Finally, the pH value of the solution was adjusted to be 7. The resultant white colloidal solution was then filtered and then dried in atmosphere air for 2 days. The as-synthesized hydroxides were used as precursors for obtaining the $\text{Gd}_{2-x}\text{Sm}_x\text{O}_3$ nanorods. The as-synthesized products were calcined independently in air at 500, 750 and 1000 °C for an hour, in a muffle furnace pre-heated at 40 °C and with a heating rate of 5 °C/min. Nanoparticles with undoped gadolinium

hydroxide were also prepared and thermally treated under the same conditions as described previously to the sample having dopant at 5 at.%. Further, the as-synthesized and calcined products were characterized with well known tools.

2.3. Characterization techniques

The phase identification and lattice parameters estimation were carried out by using powder X-ray diffraction pattern using Ultima III Rigaku X-ray diffractometer at a scanning rate of $0.02^\circ/\text{min}$ in the range of 10° – 80° with $\text{Cu-K}\alpha_1$ radiation (1.5406 \AA). The chemical compositions of the samples were identified from Fourier transform infrared (FT-IR) spectra. FT-IR spectra were recorded by using Perkin Elmer Spectrum-1: FT-IR spectrometer between the ranges of 4000 – 450 cm^{-1} . The FT-Raman spectra were recorded between 4000 and 50 cm^{-1} using BRUKER RFS-27: Stand alone FT-Raman spectrometer attached with Nd:YAG laser source. The simultaneous TG/DTA thermal analyses were carried out on the fine white powders using EXSTAR6200 TG/DTA analyzer. The TG/DTA thermograms were recorded at a scan rate of $10 \text{ }^\circ\text{C}/\text{min}$ in a flux of nitrogen gas. The particles morphology and presence of the compounds in the corresponding samples were observed using a scanning electron microscope (SEM FEI Quanta FEG 200) equipped with an energy-dispersive X-ray (SEM/EDX) micrograph.

The particle size and topography of the products were inspected using a high-resolution transmission electron microscope (HRTEM) (TECNAI G²T30, U-TWIN) with a LaB₆ filament operated at 50 – 300 kV . For TEM sample preparation, an amorphous carbon coated copper grid was placed onto a Whatman filter paper. The corresponding fine powder samples were dispersed in ethanol and then casted single drop over the copper grid by using a micropipette. The absorption spectra and band gap energy of the samples were observed and estimated using Cary 5E UV-Vis-NIR Spectrophotometer. For UV-Vis absorption spectra, the powder samples were dispersed in ethanol under sonication for 10 min. The photoluminescence (PL) emission spectra were recorded with a Perkin Elmer-LS55-luminescence spectrometer equipped with a Xe lamp as an excitation source at room temperature. X-ray photoelectron spectroscopy (XPS) measurements were carried out using an Omicron XPS instrument equipped with a hemispheric analyzer and a monochromatized Al K _{α} photon (1486.7 eV) source. Si (100) substrates for XPS measurements were cleaned for 10 min in a 5:1:1 mixture of Milli-Q water, 25% hydrogen peroxide and 30% ammonia at $80 \text{ }^\circ\text{C}$ and rinsed in Milli-Q water. All peak positions were calibrated according to the position of the carbon (C 1 s) peak. All measurements were performed at room temperature.

3. Results and discussion

3.1. Structure determination

The crystallinity and phase purity of the as-synthesized Sm:Gd(OH)₃ nanophosphors and calcined Sm:Gd₂O₃ nanophosphors were examined by the wide-angle powder XRD patterns, as shown in Fig. 1. The XRD pattern for as-synthesized Sm:Gd(OH)₃ nanophosphors [Fig. 1(a)], indicates the formation of the as-synthesized products which can be directly indexed to a hexagonal phase of Gd(OH)₃ phosphor. The diffracted peaks are in good agreement with the standard positions from JCPDS file no. 83-2037, space group: *P6₃/m* (176) [19]. The 2θ values for the intense diffraction peaks are 16.36° , 28.53° , 29.71° , 33.06° , 38.04° , 41.65° , 44.22° , 50.49° , 50.52° , 51.26° , 53.44° , 59.02° , 61.69° , 61.71° , 64.95° , 66.64° , 69.34° , 69.36° , 74.22° and 76.64° , corresponding to the (100), (110), (101), (200), (111), (201), (210), (300), (002), (211), (102), (112), (310), (202), (221), (400), (212), (302) and (230) planes, respectively. The calculated lattice parameters of the as-synthesized Sm:Gd(OH)₃ nanophosphors are $a = b = 0.6253 \text{ nm}$ and $c = 0.3612 \text{ nm}$. The hexagonal structure was transformed to pure cubic structure by different calcination processes above $500 \text{ }^\circ\text{C}$ temperature for 1 h. The cubic structure of Sm:Gd₂O₃ nanophosphors can be seen in Fig. 1(b) for $500 \text{ }^\circ\text{C}$, (c) for $750 \text{ }^\circ\text{C}$ and (d) for $1000 \text{ }^\circ\text{C}$ about 1 h. The structure transformation from hexagonal to cubic phase is in good agreement with that of JCPDS file no. 86-2477 with space group: *Ia-3* (206), [20].

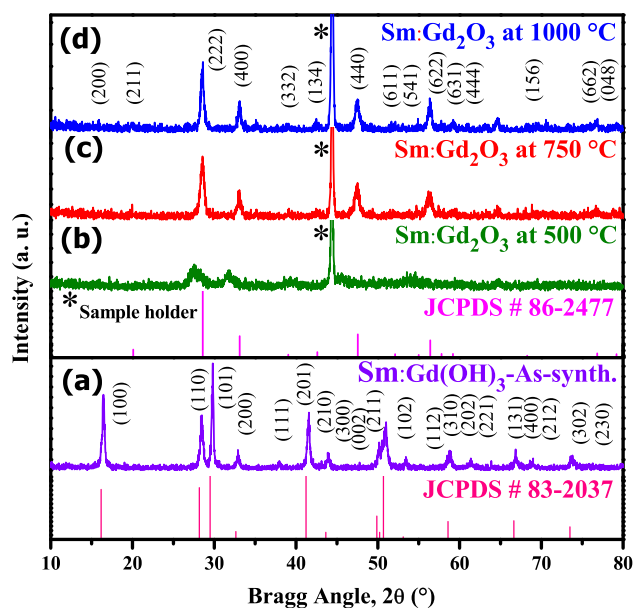


Fig. 1 Powder XRD patterns of (a) as-synthesized Sm:Gd(OH)₃ nanophosphors and calcined Sm:Gd₂O₃ nanophosphors at (b) 500, (c) 750 and (d) 1000 °C for 1 h

The intensity of these peaks was found to increase when samples were calcined at higher temperatures due to much better crystallization; however, diffraction peaks were broadened at lower calcination treatment of 500 °C for 1 h.

The lattice parameters of the cubic Sm:Gd₂O₃ nanophosphors were calculated. On the basis of the (222) crystal plane, the calculated lattice constants are $a = 1.0726$ nm for cubic phase Sm:Gd₂O₃ nanophosphors at 500 °C ($d = 3.0963$ Å), $a = 1.0824$ nm for Sm:Gd₂O₃ nanophosphors at 750 °C ($d = 3.12462$ Å) and $a = 1.1228$ nm for Sm:Gd₂O₃ nanophosphors at 1000 °C ($d = 3.2412$ Å) for about 1 h. It is worthy to note that the lattice constants of cubic structure Sm:Gd₂O₃ nanophosphors are increasing with increasing calcination temperatures. No obvious shifting of peaks or secondary phases can be detected at the doping level, indicating that the Sm³⁺ ions are completely dissolved in the Gd₂O₃ host lattices.

Sm³⁺ ions are expected to substitute for the Gd³⁺ sites due to their similar ionic radii (6 coordinate: Gd³⁺, $r = 1.078$ Å; Sm³⁺, $r = 1.098$ Å). The different crystal structures result in different magnetic and optical properties of Gd₂O₃ [21]. The peaks of carbon and nitrogen elements were not detected, indicating that the impurity absorbed from air could be removed completely and the as-synthesized Sm:Gd(OH)₃ nanophosphors have been converted to Sm:Gd₂O₃ nanophosphors during the calcination processes, which are also consistent with the FT-IR results. Strong XRD peaks of as-synthesized and calcined nanorods demonstrate the high crystallinity of the phosphors synthesized in co-precipitation technique.

3.2. Thermal behaviors of Sm:Gd(OH)₃ nanophosphors

Thermogravimetric and differential thermal analyses of as-synthesized Sm_xGd_{1-x}(OH)₃ sample are illustrated in Fig. 2. This figure illustrates the thermal decomposition of Sm_xGd_{1-x}(OH)₃ sample proceeds in temperature ranges of 34–1000 °C under ambient pressure. At 320 °C a strong endothermic peak is observed in the DTA curve that corresponds to the main weight loss of 9.2% indicating the formation of Sm_xGd_{2-x}O₃. The TG studies of the thermal transformation of the sample govern four steps of weight loss. The first (I) step in temperature range from 34 to 261 °C is observed with weight loss of 2.6%. This weight loss corresponds to the evaporation of moisture and a partial dehydration of water content in the sample. The second (II) step weight loss 7.9% is observed between 261 and 329 °C temperatures. This weight loss belongs to the complete dehydration of residual water on the surface of the sample. The weight loss 2.8% in the range from 329 to 456 °C is observed in the third (III) step of thermal transformation. The endothermic peak at 329 °C may be correlated to the transformation of Sm_xGd_{1-x}(OH)₃ phase

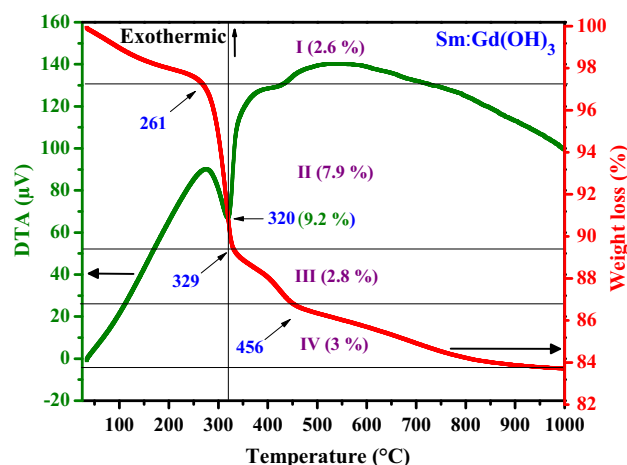
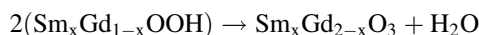


Fig. 2 TG/DTA curve of Sm:Gd(OH)₃ nanophosphors

to the intermediate Sm_xGd_{1-x}OOH phase. The third (III) step leads to the gradual weight loss, which is the initial stage for the formation of Sm_xGd_{2-x}O₃ phase.

The fourth (IV) step with weight loss of 3% in between the ranges of 456–1000 °C is observed. This weight loss corresponds to the further formation of Sm_xGd_{2-x}O₃. The proposed reaction mechanism can be described by the following expressions,



Hence, thermal analyses suggest that the presence of moisture absorbed from the atmosphere and hydroxide phase of samarium doped gadolinium in the as-synthesized sample. This causes the further change into Sm_xGd_{2-x}O₃ phase on calcination process above 500 °C temperature. Thus there were three samples, (1) as-synthesized, (2) calcined at 500 °C for 1 h and (3) calcined at 750 °C for 1 h, considered for the further studies.

3.3. FT-Raman and FTIR spectroscopy

Raman spectroscopy is an important and informative tool to elucidate the structure of the as-synthesized and calcined samples. Figure 3(i) shows the room temperature FT-Raman spectra of (a) as-synthesized Sm:Gd(OH)₃, (b) Sm:Gd₂O₃ at 500 °C and (c) Sm:Gd₂O₃ at 750 °C for 1 h. FT-IR spectra of the as-synthesized Sm:Gd(OH)₃ and calcined Sm:Gd₂O₃ samples are presented in Fig. 3(ii) (a), (b), respectively. It is known that the presence of –OH and –CO vibrational groups in phosphor materials can also quench or reduce the luminescence intensity [22].

According to the factor group theory analyses [23], 22 Raman modes have been predicted for the body-centered C-type cubic structure Gd₂O₃. These modes are expected to be 4A_g, 4E_g and 14F_g Raman active modes. In the present

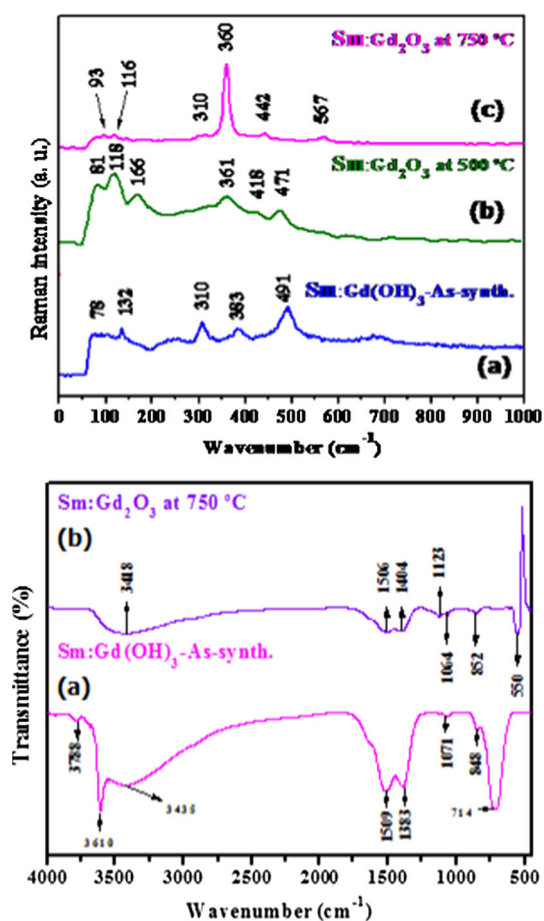


Fig. 3 (i) FT-Raman spectra of as-synthesized (a) Sm:Gd(OH)₃ and calcined Sm:Gd₂O₃ nanophosphors at (b) 500 and (c) 750 °C for 1 h. (ii) FT-IR spectra of (a) as-synthesized Sm:Gd(OH)₃ and (b) calcined Sm:Gd₂O₃ nanorods at 750 °C for 1 h

work, some of the Raman modes were not detected as reported in the literature [24]. This may be attributed several conditions such as preparation technique, type of phase formation and the impurity (Sm) present in the samples, etc. The broad and more intense band at 491 cm⁻¹ along with less intense bands at 78, 132, 310 and 383 cm⁻¹ were observed in Fig. 3(a). The peak at 491 cm⁻¹ (A_g mode) has been assigned as the hexagonal structure of Sm:Gd(OH)₃.

For Sm:Gd₂O₃ sample calcined at 500 °C [Fig. 3(i) (b)] and at 750 °C [Fig. 3(c)], the weak peak at 361 cm⁻¹ along with medium intense peaks at 418 and 471 cm⁻¹ and the strong peak 360 cm⁻¹ along with the weak intense peaks at 310, 442 and 567 cm⁻¹ are observed respectively. These peaks mainly are assigned to C-type cubic phase Gd₂O₃. As seen in Fig. 3(b), (c), the measured Raman bands indicate that a large polarizability change during the vibration. Zhang et al. [25] have reported that the reduction in crystalline dimension to the nanometer range can cause the frequency shift and the broadening of Raman peaks as a

result of phonon confinement. The full width at half maximum of the peak at 360 cm⁻¹ for Sm:Gd₂O₃ increases with increasing the calcination temperatures. This case leads to a considerable reduction in the structural order and crystallinity which were also evidenced from the powder XRD results. There is no impurity (Sm) characteristic peak was observed in the corresponding as-synthesized and calcined samples, confirms the single phase nature occurred in the samples. On the other hand, these results recorded from the FT-Raman spectra conclude that the samarium dopant was completely dissolved into the gadolinium sites as its ionic radii is almost close to gadolinium ion.

As shown in Fig. 3(ii) (a), the weak and strong bands observed in FTIR spectra at 3788 and 3610 cm⁻¹ which are ascribed to the O–H stretching vibration of adsorbed water molecule and Gd–O–H stretching vibration, respectively [26]. The band at about 3435 cm⁻¹ is also due to –OH stretching vibration of adsorbed water from air. The strong bands at 1509 and 1383 cm⁻¹ are due to C–O band of carbon-dioxide from the atmosphere during the pellet preparation for IR measurements. The absorption peaks of the CO₃²⁻ anion groups at 1071 and 848 cm⁻¹ have been observed. The IR band at 714 cm⁻¹ corresponds to –C–H out-of-plane vibration.

In Fig. 3(ii) (b), the peak at 3418 cm⁻¹ is due to O–H stretching vibration. A decrease in intensity of the band at 3418 cm⁻¹ is observed for calcined Sm:Gd₂O₃ sample when compared with the as-synthesized Sm:Gd(OH)₃ sample. The band appearing at 1506, 1404, 1123–1064 and 852 cm⁻¹ can be assigned to CO asymmetric stretching, CO asymmetric stretching, CO symmetric stretching and CO deformation vibrations respectively, suggest the composition of the corresponding sample. A new band centered at about 550 cm⁻¹ can be attributed to the Gd–O stretching frequency of cubic Sm:Gd₂O₃ [27]. On the basis FT-IR results it can further inferred that the samples are essentially free of the nitrate-group (2213–2034 cm⁻¹). It is clearly seen that the bands at 3610 and 714 cm⁻¹ for as-synthesized Sm:Gd(OH)₃ sample, disappeared quite in calcined Sm:Gd₂O₃ sample obtained at 750 °C for 1 h. These results suggesting that the Sm:Gd(OH)₃ sample had transformed to Sm:Gd₂O₃ structure after the calcination treatment. The results are consistent with that of the powder XRD patterns.

3.4. Scanning electron microscopy (SEM) studies

The formation of 1-D structure can be explained by the self or induced scrolling mechanism [28]. Figure 4(a)–(d), represent the SEM images of the calcined Sm:Gd₂O₃ nanorods at 750 °C for 1 h, with an energy dispersive X-ray analysis. The observed Sm:Gd₂O₃ nanorods are in

diameters ranging from 70–150 nm and lengths ranging from 210–520 nm.

It can be seen that the calcined Sm:Gd₂O₃ nanorods inherit their parents' morphology, but their size is significantly varied in comparison with the Sm:Gd(OH)₃ nanorods in that the density of the former is higher than that of the latter. The Sm:Gd(OH)₃ nanorods were converted to Sm:Gd₂O₃ during the subsequent calcination process with gradual elimination of H₂O. Nevertheless, the conversion did not lead to the change in the morphology. Such a transformation was common for a lanthanide hydroxide compound decomposing [29]. From EDX [Fig. 4(d)], the presence of samarium as dopant was found to be around 5 at.% which is in close agreement with the composition that was initially assigned.

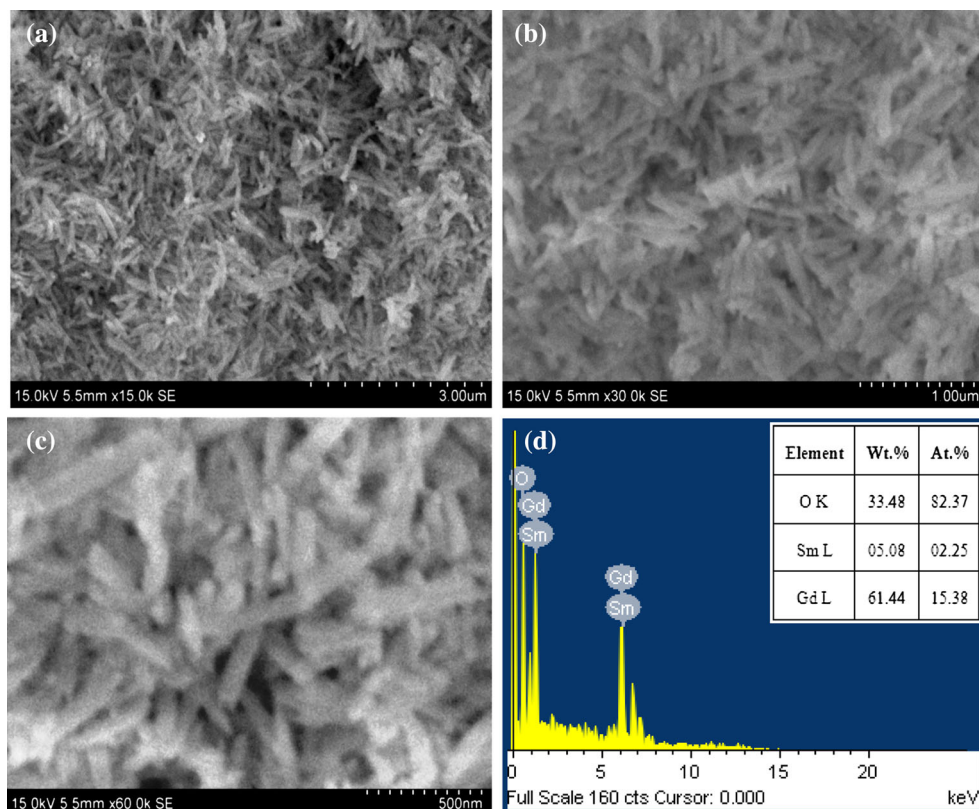
3.5. Transmission electron microscopy (TEM) studies

A typical TEM images of Sm:Gd(OH)₃ phosphor revealed that the well-resolved bundle of rod-like morphology. These bundles of nanorods were formed by self assembling many small size nanorods. Tso [30] and Hunter [31] reported that in the enzymatic precipitation (EP) method, the enzyme urease was used to decompose urea at room temperature, releasing NH⁴⁺ that reacts as a precipitant; EP particles of less than 100 nm in diameter show a high tendency to form agglomerates [32].

Phase purity and crystalline order are recognized as two most important parameters which significantly influence the properties of nanomaterials [19]. Figure 5(a), (b) presents the TEM images of calcined Sm:Gd₂O₃ nanorods obtained at 750 °C for 1 h. It can be observed these nanostructures demonstrate rod-like morphology with a length in the range of about 110–420 nm and the diameter of 40–90 nm. It also reveals that these one-dimensional nanostructures have tapered end and defect surface as shown in Fig. 5(a), (b). It is evident that the Sm:Gd₂O₃ nanorods maintain the anisotropic shape during heat-treatment from 500–750 °C for 1 h. It also can be observed that the formation of nanorods is attributed to the fact that the growth direction are preferred along the [222] crystallographic orientation.

This is because the interplanar spacing between the fringes along nanorod axes is about 0.3124 nm which is close to the interplanar distance of the cubic (222) plane as presented in Fig. 8(c). The aspect ratio calculated for 750 °C calcined Sm:Gd₂O₃ nanorods was about greater than 5. This aspect ratio value is more than the 500 °C calcined Sm:Gd₂O₃ nanorods but less the as-synthesized Sm:Gd(OH)₃ nanorods.

Fig. 4 SEM micrographs of calcined Sm:Gd₂O₃ nanorods at different magnifications [(a)–(c)] with EDX analysis (d) at 750 °C for 1 h



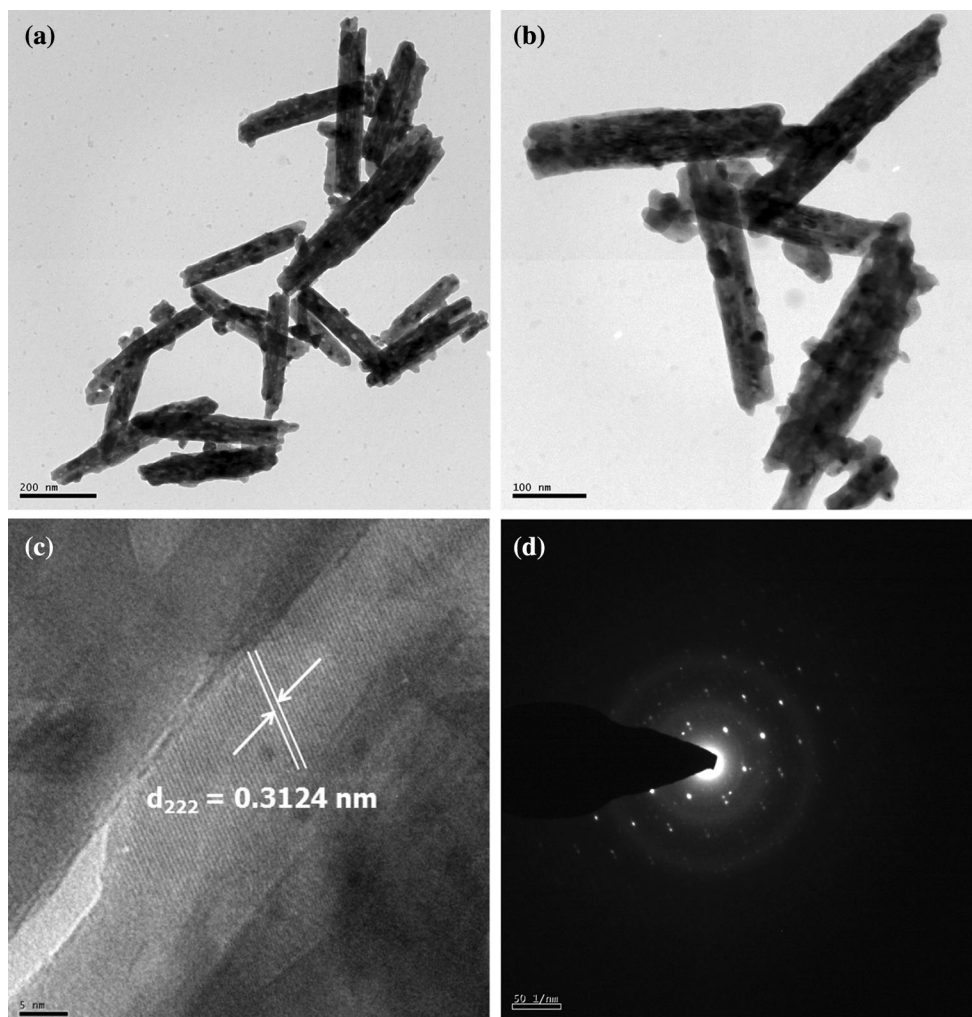


Fig. 5 TEM images of calcined Sm:Gd₂O₃ nanorods at different magnifications [(a)–(c)] with SAED pattern analysis (d) at 750 °C for 1 h

3.6. Absorbance and photoluminescence studies

Figure 6(a), (b) illustrate the UV–Vis absorption and PL emission spectra of the as-synthesized Sm:Gd(OH)₃ and calcined Sm:Gd₂O₃ nanorods at 750 °C for 1 h. The UV–Visible absorbance spectra of Sm:Gd(OH)₃ and Sm:Gd₂O₃ nanorods consisting strong absorption bands centered at about 207 nm and 234 nm, are shown in Fig. 6(a), (b), respectively. However, it is observed from Fig. 6(a), the several weak absorption bands are found in Sm:Gd(OH)₃ nanorods. The broad and strong PL emission band at 412 nm was obtained by using the absorption wavelength as an excitation wavelength. Similarly, an intense and sharp PL emission band at 393 nm was observed by exciting a wavelength of absorbance around 240 nm. Even though the PL emission is shifted towards lower region of visible region [Fig. 6(b)], the intensity of the Sm:Gd₂O₃ nanorods is enormously increased due to the calcination temperature which can be seen in Fig. 6. The large Stokes' shift (~ 160 nm) observed in Sm:Gd₂O₃ nanorods is

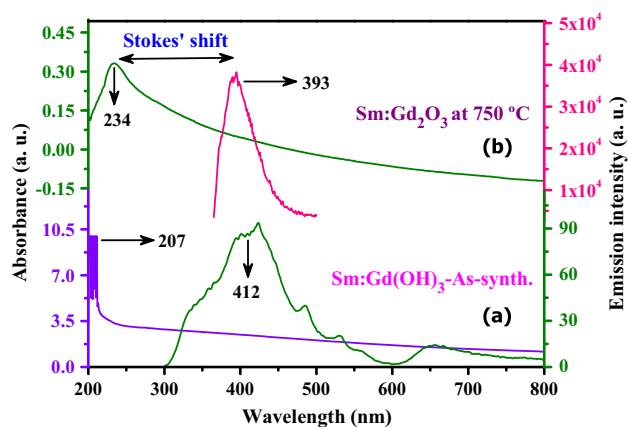


Fig. 6 UV–Vis absorption and photoluminescence emission spectra of (a) as-synthesized Sm:Gd(OH)₃ and (b) calcined Sm:Gd₂O₃ nanorods at 750 °C for 1 h

shown in Fig. 6(b). It is worth to note that the materials with large Stokes' shift are also optimal matrix for fluorescent solar concentrator devices [33].

There may be some structural defects in the as-synthesized Sm:Gd(OH)₃ nanorods but still it is possible to reduce the disorder when increasing the calcination temperature. Hence, if the structure becomes more ordered with the heat treated temperature (i.e. when the concentration of structural defects such as oxygen vacancies), distortions and/or strains in the lattice are reduced. According to Tauc plot expression, the band gap energies for Sm:Gd(OH)₃ and Sm:Gd₂O₃ nanorods (Fig. 7) were evaluated to be 4.37 and 4.46 eV, respectively. Adachi et al. [34] has reported the band gap energy values for undoped Gd₂O₃ nanoparticles in the range of 5.0–5.6 eV. But in our work, we have found it to be 4.46 eV. The sample preparation methods and reaction conditions may vary the band gap energies of gadolinium oxide. The difference between the band gap energies of samarium doped gadolinium oxide nanorods and undoped gadolinium oxide nanoparticles was found to be 0.28 eV which led to the band gap narrowing presence in Sm:Gd₂O₃ nanorods.

The presence of intermediary energy levels (deep and shallow holes) is minimized within the optical band gap and consequently, the E_g values increase. Moreover, it is interesting that the sharp and highly intense violet color was observed in PL emission spectrum of Sm:Gd₂O₃ nanorods. In addition to this case, the PL emission spectrum of the undoped Gd₂O₃ nanoparticles constituting a broad band along with many weak bands when compared to samarium doped gadolinium oxide nanorods. Thus, these results revealed that the doping effect into the host lattice is influenced in enhancing the luminescence intensity.

The emission spectra for 400 nm is given in below Fig. 8. For the excitation wavelength of 400 nm we do not observe any splitting in ⁵D₀–⁷F₂ transition as shown in Fig. 8. The cubic structure of Sm³⁺ in the lanthanides may be the reason for the absence of splitting at this excitation for our present investigation. In the site occupancy of C₂

and S6 sites, Gd³⁺ ions occupy 75:25%. In this the emission originates from the C₂ symmetry in which there is no centre of inversion and hence we do not observe any splitting. The other transitions do not appear in the spectrum as it merges in the convolution and broadened nature of the curve.

3.7. X-ray photoelectron spectroscopy (XPS) analyses

The chemical composition of the Sm:Gd₂O₃ nanorods was carried out with X-ray photoelectron spectroscopy (XPS). The experimental data were analyzed using the CASA-XPS software. The high-resolution spectra of gadolinium (3d) and gadolinium (4d), are presented in Figs. 9 and 10, respectively. The wide-scan survey spectrum of calcined Sm:Gd₂O₃ nanorods was recorded in the binding energy range of 0–1300 eV. The inelastic mean free path of an electron is independent on its kinetic energy according to the Universal curve [35]. The experimental gadolinium/oxygen ratio, as calculated from the total areas of Gd (3d) and O (1s) peaks in the wide-scan survey spectrum, were estimated to be 1.79 corresponds to [Gd 3d_{5/2}]/[O (1s)] and 1.31 corresponds to [Gd 3d_{3/2}]/[O (1s)].

A high-resolution XPS spectrum of Gd (3d) spin–orbit doublet of Sm:Gd₂O₃ nanorods are shown in Fig. 9. The peak positions of the Gd (3d) emission line in the Sm:Gd₂O₃ nanorods have the binding energy values for Gd 3d_{5/2} = 1188.46 eV and for Gd 3d_{3/2} = 1220.85 eV. But the standard elemental binding energy values of Gd 3d_{5/2} and Gd 3d_{3/2} are to be 1186 and 1218 eV, respectively. Thus, it is clear that the observed binding energy values of Gd (3d) lines were shifted to the higher binding energy values. These two levels are separated with an energy difference of binding energy around 32 eV, confirms that the Gd characterizes its Gd³⁺ oxidation state. Figure 10 shows the peak positions of Gd (4d) spin–orbit splittings in Sm:Gd₂O₃ nanorods. The selection rules predict that the

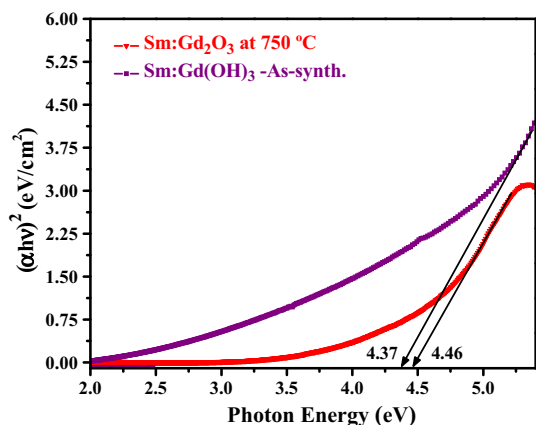


Fig. 7 Energy band gap of (a) as-synthesized Sm:Gd(OH)₃ and (b) calcined Sm:Gd₂O₃ nanorods at 750 °C for 1 h

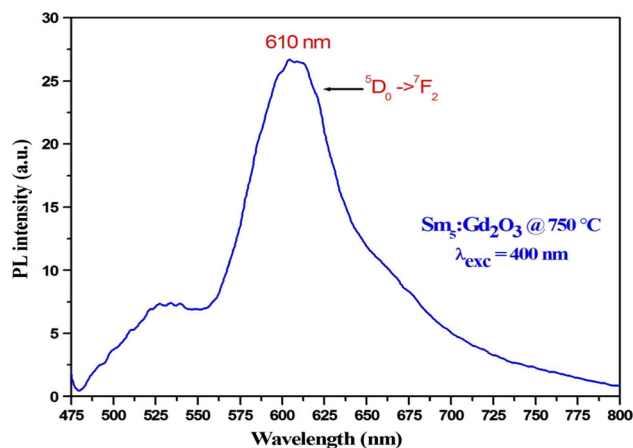


Fig. 8 PL spectra of Sm:Gd₂O₃ calcinated at 750 °C

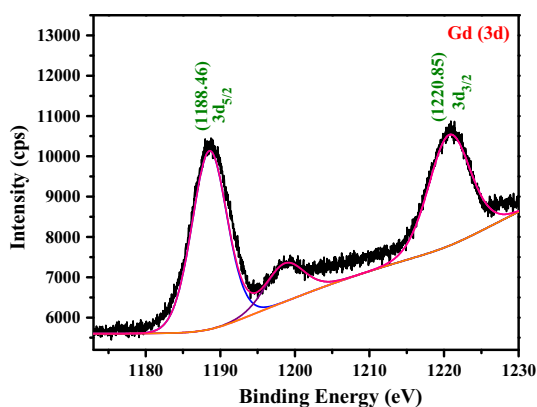


Fig. 9 Gd (3d) HRXPS spectrum of Sm:Gd₂O₃ nanorods at 750 °C for 1 h

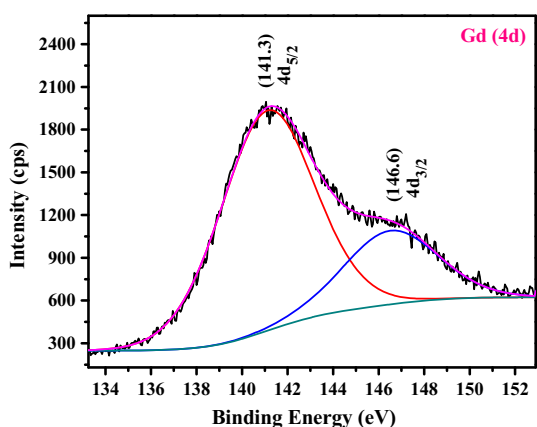


Fig. 10 Gd (4d) HRXPS spectrum of Sm:Gd₂O₃ nanorods at 750 °C for 1 h

highest splitting lies in the lowest binding energy values and the lowest splitting lies in the highest binding energy values. Thus, the binding energy values of Gd 4d_{5/2} and Gd 4d_{3/2} are found to be 141.3 and 146.6 eV, respectively [36].

Similar to the (As the) Gd (3d) emission line, these two levels of Gd (4d) are separated with a small energy difference in their binding energy values. The evaluated difference comes to 5.3 eV. Hence, it can be confirmed that the peak position of Gd (4d) characterized the Gd³⁺ oxidation state. The curve shape and peak positions are matched well with the earlier values reported in literature [37].

4. Conclusions

The effect of samarium substitution on the gadolinium hydroxide and its oxide were investigated by using various characterization techniques such as X-ray diffraction, FT-Raman spectroscopy, scanning electron microscopy, transmission electron microscopy, photoluminescence and X-ray photoelectron spectroscopy. The transition

temperature of Sm:Gd(OH)₃ to Sm:Gd₂O₃ was confirmed by TG/DTA analysis. It was also confirmed by the XRD measurements. The structural phase transition of Sm:Gd(OH)₃ to Sm:Gd₂O₃ was confirmed by FT-Raman scattering which was supported with the XRD results. Similar to the previously observed dopant effect, samarium doped samples in the present work was also exhibiting the rod-like morphology which was evidenced from SEM and TEM measurements. Further, the analysis of HRTEM fringe pattern ($d_{222} = 0.3124$ nm) of Sm:Gd₂O₃ nanorods confirms its (222) orientation, which is the orientation of hundred percentage peak of XRD. The band gap energy estimation of both the samples confirm the red-shift (0.1 eV) because of the temperature induced transformation of Sm:Gd(OH)₃ and Sm:Gd₂O₃ nanorods. Its influence was also observed in photoluminescence spectra. From the difference between the absorption maximum and photoluminescence maximum, the Stokes' shift was estimated and it was found to be 159 nm. These preliminary investigations provide a fruitful result for its use in luminescent applications.

References

- [1] A Garcia-Murillo, C L Luyer-Urlacher, C Dujardin, C Pedrini and J Mugnier *J. Sol-Gel Sci. Technol* **26** 957 (2003)
- [2] M Buijs, A Meyerink and G Blasse *J. Lumin.* **37** 9 (1987)
- [3] L Fornasiero, E Mix, V Peters, K Petermann and G Huber *Cryst. Res. Technol.* **34** 255 (1999)
- [4] S K Singh, K Kumar and S B Rai *Sens. Actuators A Phys.* **149** 16 (2009)
- [5] X Wang and Y Li *Angew. Chem. Int. Ed.* **41** 4790 (2002)
- [6] Y Xue, J Li, W Ma, Y Zhou and M Duan *J. Mater. Sci.* **41** 1781 (2006)
- [7] A W Xu, Y P Fang, L P You and H Q Liu *J. Am. Chem. Soc.* **125** 1494 (2003)
- [8] W O Gordon, J A Carter and B M Tissue *J. Lumin.* **108** 339 (2004)
- [9] M L Debasu, D Ananias, A G Macedo, J Rocha and L D Carlos *J. Phys. Chem. C* **115** 15297 (2011)
- [10] C K Duan, M Yin, K Yan and M Reid *J. Alloys Compd.* **303** 371 (2000)
- [11] N Sammes and Y Du *NATO Sci. Ser.* **202** 19 (2005)
- [12] M Buijs, A Meyerink and G Blasse *J. Lumin.* **37** 9 (1987)
- [13] B Bihari, H Eilers and B M Tissue *J. Lumin.* **75** 1 (1997)
- [14] M J Treadaway and R C Powell *Phys. Rev.* **B 11** 862 (1975)
- [15] J B Gruber, B Zandi and M F Reid *Phys. Rev.* **B 60** 15643 (1999)
- [16] H A Kramers *Proc. Amst. Acad.* **33** 959 (1930)
- [17] L T Su, A I Y Tok, F Y C Boey, X H Zhang, J L Woodhead and C J Summers *J. Appl. Phys.* **102** 083541 (2007)
- [18] L Li, H K Yang, B K Moon, B C Choi, J H Jeong and K H Kim *Mater. Chem. Phys.* **119** 471 (2010)
- [19] Z Liu, F Pu, S Huang, Q Yuan, J Ren and X Qu *Biomaterials* **34** 1712 (2013)
- [20] N Dhananjaya, H Nagabhushana, B M Nagabhushana, B Rudraswamy, C Shivakumara and R P S Chakradhar *Physica B* **406** 1639 (2011)
- [21] R M Moon and W C Koehler *Phys. Rev. B* **11** 1609 (1975)

- [22] J A Capabianco, J C Boyer, F Vetrone, A Speghini and M Bettineli *Chem. Mater.* **14** 2915 (2002)
- [23] W B White and V G Keramidas *Spectrochim. Acta A* **28** 501 (1972)
- [24] N Dilawar, S Mehrotra, D Varandani, B V Kumaraswamy, S K Haldar, A K Bandyopadhyay, *Mater. Charact.* **59** 462 (2008)
- [25] W F Zhang, Y L He, M S Zang, Z Yin and Q Chen *J. Phys. D* **33** 912 (2000)
- [26] Q Mu, T Chen and Y Wang *Nanotechnology* **20** 345602 (2009)
- [27] A Garcia-Murillo, C L Luyer, C Dujardin, C Pedrini and J Mugnier *Opt. Mater.* **16** 39 (2001)
- [28] C Chang, F Kimura, T Kimura and H Wada *Mater. Lett.* **59** 1037 (2005)
- [29] J X Wan, Z H Wang, X Y Chen, L Mu and Y T Qian *J. Cryst. Growth* **284** 538 (2005)
- [30] C Tso, C Zhung, Y Shih, Y M Tseng, S Wu and R Doong *Water Sci. Technol.* **61** 127 (2010)
- [31] R J Hunter *Foundations of Colloid Science* (New York: Oxford University Press) (2001)
- [32] E Matijevic and W P Hsu *J. Colloid Interface Sci.* **118** 506 (1987)
- [33] F Vollmer, W Rettig and E Birekner *J. Fluoresc.* **4** 65 (1994)
- [34] G Adachi and N Imanaka *Chem. Rev.* **98** 1479 (1998)
- [35] G Attard and B Colin *Surfaces* (New York: Oxford Chemistry Primers, Oxford University Press) (1998)
- [36] J F Watts and J Wolstenholme *An Introduction to Surface Analysis by XPS and AES* (Chichester: Wiley) (2003)
- [37] D Raiser and J P Deville *J. Electron Spectrosc. Relat. Phenom.* **57** 91 (1991)